PHYSICAL REVIEW D **96,** 044043 (2017)

Scalar absorption by charged rotating black holes

Luiz C. S. Leite,[*] Carolina L. Benone,[†] and Luís C. B. Crispino[‡]
Faculdade de Física, Universidade Federal do Pará, 66075-110 Belém, Pará, Brazil
(Received 16 April 2017; published 30 August 2017)

We compute numerically the absorption cross section of planar massless scalar waves impinging upon a Kerr-Newman black hole with different incidence angles. We investigate the influence of the black hole electric charge and angular momentum in the absorption spectrum, comparing our numerical computations with analytical results for the limits of high and low frequency.

DOI: 10.1103/PhysRevD.96.044043

I. INTRODUCTION

The existence of black holes (BHs) has been intensively debated for many decades. Although a lot of indirect evidence that BHs are present in nature has been collected, e.g., Cygnus X-1 [1], BHs still demanded stronger evidence of their existence. The recent report of the detection of gravitational waves [2,3] is remarkable, not only for the confirmation of one of the most important predictions of general relativity (GR) but also because the gravitational waves detected by LIGO Scientific Collaboration are claimed to have been produced by the merger of a binary BH system, providing additional evidence that BHs indeed exist in nature.

One way to investigate the nature of BHs is by observing how they absorb/scatter particles and waves in their vicinity. In this context, many works have been done in order to determine the absorption and scattering cross sections of BHs, considering different BH solutions, particles, and waves of different kinds. Using numerical techniques, Sanchez investigated the absorption and scattering of planar massless scalar waves by a Schwarzschild BH [4,5], taking a first step in this line of investigation. The absorption and scattering cross sections have also been studied for the case of Reissner-Nordstrom BHs [6–15], Kerr BHs [16–18], and regular BHs [19,20]. Recently, the absorption of massless scalar waves by a Schwarzschild BH surrounded by a thin shell of matter has also been analyzed [21]. However, the absorption and scattering of scalar waves by Kerr-Newman BHs has not been investigated yet.

Massless scalar waves can be seen as a simpler proxy for higher-spin waves, such as the electromagnetic and gravitational waves. In addition to that, recently, it was proposed that ultralight bosons with null spin can be good candidates of dark matter [22,23]. Such fields, which are called fuzzy dark matter, would interact with black holes, for instance at the core of galaxies; so, it is of interest to study how these fields are scattered and absorbed by the black hole.

We can wonder if it is reasonable to assume a black hole to have a nonzero electric charge. The electromagnetic force can lead to the discharge of a black hole, favoring (disfavoring) charges of opposite (the same) sign of the black hole charge to be absorbed. Another phenomenon to take into consideration is the emission of particles by black holes [24]. Charged black holes tend to emit more particles with the same charge sign of the black hole than with the opposite sign, also leading to a neutralization of the black hole [25]. However, in the context of minicharged dark matter [26], it is possible to have black holes with a considerable amount of charge and even extremely charged black holes [27].

While investigating the scattering of fields by chargeless rotating BHs, one finds that for small enough frequencies the scattered wave can be amplified, decreasing the energy and angular momentum of the black hole. Such a phenomenon is known as superradiance, and it was first investigated by Misner [28]. Moreover, Hawking radiation brought extra motivation to the study of the absorption cross section of BHs, since the emission rate of a BH is proportional to its absorption cross section.

In this work, we consider the case of a massless scalar plane wave impinging upon a rotating and charged BH, computing the absorption cross section numerically. In the low-frequency limit, we consider the general result obtained by Higuchi [29], and for the high-frequency limit, we consider the eikonal approach, using the geodesic equation to obtain the high-frequency absorption cross section. This paper is organized as follows. In Sec. II, we present the Kerr-Newman metric written in Boyer-Lindquist coordinates and make a brief review of the treatment given to the massless scalar field in the Kerr-Newman background. In Sec. III, we present expressions for the absorption cross section, which are obtained via the partial-wave approach. In Sec. IV, we exhibit our numerical results for different choices of the plane wave incidence angle, the rotation parameter and the electric charge of the BH. We finish this paper by presenting some remarks in Sec. V. We adopt natural units ($c = G = \hbar = 1$).

[*]luizcsleite@ufpa.br
[†]lben.carol@gmail.com
[‡]crispino@ufpa.br

II. SCALAR FIELD IN THE KERR-NEWMAN SPACETIME

In standard Boyer-Lindquist coordinates $\{t, r, \theta, \phi\}$, the Kerr-Newman BH is described by the following line element,

$$ds^2 = \left(1 - \frac{2Mr - Q^2}{\rho^2}\right)dt^2 - \frac{\rho^2}{\Delta}dr^2 - \rho^2 d\theta^2 + \frac{4Mar\sin^2\theta - 2aQ^2\sin^2\theta}{\rho^2}dt d\phi - \frac{\xi\sin^2\theta}{\rho^2}d\phi^2, \tag{1}$$

where we have defined $\rho^2 \equiv r^2 + a^2\cos^2\theta$, $\Delta \equiv r^2 - 2Mr + a^2 + Q^2$, and $\xi \equiv (r^2 + a^2)^2 - \Delta a^2\sin^2\theta$. The set of parameters (M, Q, a) is interpreted, respectively, as the mass, the electric charge, and angular momentum per unit mass of the BH. The Kerr-Newman metric represents a BH spacetime such that $a^2 + Q^2 \leq M^2$. Here, we shall restrict our attention to the case $a^2 + Q^2 < M^2$, which presents two distinct horizons, namely, an internal (Cauchy) horizon located at $r_- = M - \sqrt{M^2 - a^2 - Q^2}$ and an external (event) horizon at $r_+ = M + \sqrt{M^2 - a^2 - Q^2}$.

A massless scalar field $\Psi(x^\mu)$ is governed by the Klein-Gordon equation, which can be written in its covariant form as

$$\frac{1}{\sqrt{-g}}\partial_\mu(\sqrt{-g}g^{\mu\nu}\partial_\nu\Psi) = 0, \tag{2}$$

where $g_{\mu\nu}$ are the covariant components of the Kerr-Newman metric, which can be obtained directly from Eq. (1). $g^{\mu\nu}$ are the contravariant components of the metric, and g is the metric determinant.

We can decompose the scalar field in wavelike solutions of Eq. (2), as follows:

$$\Psi = \sum_{l=0}^{+\infty}\sum_{m=-l}^{+l}\frac{U_{\omega lm}(r)}{\sqrt{r^2 + a^2}}S_{\omega lm}(\theta)e^{im\phi - i\omega t}. \tag{3}$$

The functions $S_{\omega lm}$, appearing in Eq. (3), are the standard oblate spheroidal harmonics [30], which satisfy the following equation,

$$\left(\frac{d^2}{d\theta^2} + \cot\theta\frac{d}{d\theta}\right)S_{\omega lm} + \left(\lambda_{lm} + a^2\omega^2\cos^2\theta - \frac{m^2}{\sin^2\theta}\right)S_{\omega lm} = 0, \tag{4}$$

where λ_{lm} are the eigenvalues of the spheroidal harmonics. These angular functions are normalized as follows:

$$\int d\theta \sin\theta |S_{\omega lm}(\theta)|^2 = \frac{1}{2\pi}. \tag{5}$$

Using the definition of the tortoise coordinate $r_\star$ in the Kerr-Newman spacetime, namely,

$$r_\star \equiv \int dr\left(\frac{r^2 + a^2}{\Delta}\right), \tag{6}$$

the differential equation obeyed by the radial function $U_{\omega lm}$ can be rewritten as

$$\left(\frac{d^2}{dr_\star^2} + V_{\omega lm}\right)U_{\omega lm}(r_\star) = 0, \tag{7}$$

with $V_{\omega lm}$ given by

$$V_{\omega lm}(r) = \left(\omega - m\frac{a}{r^2 + a^2}\right)^2 + \left[2Mr - 2r^2 - \Delta + \frac{3r^2}{r^2 + a^2}\Delta\right]\frac{\Delta}{(r^2 + a^2)^3} - (a^2\omega^2 + \lambda_{lm} - 2ma\omega)\frac{\Delta}{(r^2 + a^2)^2}. \tag{8}$$

In Fig. 1, we plot the function $-M^2V_{\omega lm}$ for different values of the BH charge-to-mass ratio, $q \equiv Q/M$, (right panel) and rotation parameter (left panel), fixing $M\omega = 0.1$ and $l = m = 1$, in both cases. We note that the larger the BH rotation and charge are, the larger $-M^2V_{\omega lm}$ is. Moreover, $-M^2V_{\omega lm}$ presents a maximum and then goes to $-M^2\omega^2$ at infinity.

The radial Eq. (7) has a set of independent solutions usually labelled as *in, up, out*, and *down*. The in modes are the appropriate ones for studying absorption and scattering processes, since they denote purely incoming waves from the past null infinity. These modes have the following asymptotic behavior,

$$U_{\omega lm}(r_\star) \sim \begin{cases} \mathcal{I}_{\omega lm}U_I + \mathcal{R}_{\omega lm}U_I^* & (r_\star/M \to +\infty), \\ \mathcal{T}_{\omega lm}U_T & (r_\star/M \to -\infty), \end{cases} \tag{9}$$

in which

$$U_T = e^{-i(\omega - m\Omega_H)r_\star}\sum_{j=0}^{N} g_j(r - r_+)^j, \tag{10}$$

$$U_I = e^{-i\omega r_\star}\sum_{j=0}^{N}\frac{h_j}{r^j}, \tag{11}$$

and $\Omega_H \equiv \frac{a}{r_+^2 + a^2}$ is the event horizon angular velocity. The symbol * denotes complex conjugation. g_j and h_j are constants, which can be found by assuming that Eq. (9) obeys Eq. (7) in the asymptotic limits. The coefficients $\mathcal{R}_{\omega lm}$ and $\mathcal{T}_{\omega lm}$ are related to the reflection and transmission coefficients, respectively, and obey the equation

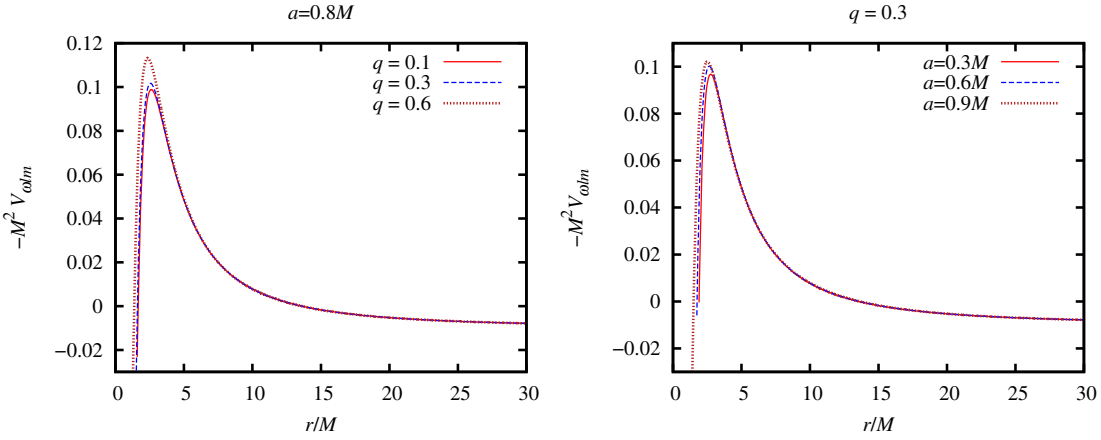

FIG. 1. LEFT: We plot $-M^2V_{\omega lm}$ as a function of r for a fixed value of the BH angular momentum, $a = 0.8M$, and different values of BH charge-to-mass ratio, $q \equiv Q/M$. RIGHT: The function $-M^2V_{\omega lm}$ is plotted for $q = 0.3$ and different values of a. For both cases, we choose $M\omega = 0.1$ and $l = m = 1$.

$$\left|\frac{\mathcal{R}_{\omega lm}}{\mathcal{I}_{\omega lm}}\right|^2 = 1 - \frac{\omega - m\Omega_{\rm H}}{\omega}\left|\frac{\mathcal{T}_{\omega lm}}{\mathcal{I}_{\omega lm}}\right|^2. \tag{12}$$

From this relation, one can see that for $0 < \omega < m\Omega_{\rm H}$, $|\mathcal{R}_{\omega lm}|^2 > |\mathcal{I}_{\omega lm}|^2$. This enhancement in the amplitude of the reflected wave is known as superradiance [31].

III. ABSORPTION CROSS SECTION

The absorption cross section can be well described by analytical approximate results in the low- and high-frequency regimes. In the low-frequency regime, it has been shown that the absorption cross section of massless scalar waves for stationary BHs, such as a Kerr-Newman BH, is given by the area of the event horizon [29]. In the high-frequency limit, the absorption cross section tends to the capture cross section of null geodesics. These limiting results are important to check the accuracy of the numerical results, which are exhibited in Sec. IV. We will show that our numerical results, both in the low- and high-frequency regimes, are in agreement with the analytical limits.

We can obtain an expression for the absorption cross section through the partial-wave approach, so that the total absorption cross section of massless scalar waves impinging upon a Kerr-Newman BH with an incidence angle γ, is

$$\sigma = \sum_{l=0}^{\infty}\sum_{m=-l}^{l}\frac{4\pi^2}{\omega^2}|S_{\omega lm}(\gamma)|^2\left(1 - \left|\frac{\mathcal{R}_{\omega lm}}{\mathcal{I}_{\omega lm}}\right|^2\right). \tag{13}$$

According to the value assumed by the azimuthal number m, we can distinguish the modes between corotating ($m > 0$) and counterrotating ($m \leq 0$) with the BH.[1] Hence, the total absorption cross section can be seen as a sum of the corotating and the counterrotating contributions allowing the splitting of the absorption cross section into superradiant modes (σ^{co}), and nonsuperradiant modes ($\sigma^{\rm counter}$), respectively [32].

A. Capture cross section

In the high-frequency regime, the absorption cross section approaches the capture cross section of null geodesics, which is given by

$$\sigma_{\rm geo} = \frac{1}{2}\int_{-\pi}^{\pi} b_c^2(\chi,\gamma)d\chi, \tag{14}$$

where χ is an angle defined in the plane of the impinging wave. When b_c is constant, we recover $\sigma_{\rm geo} = \pi b_c^2$, which is the high-frequency absorption cross section for static geometries. In Ref. [18], an approach for the computation of the capture cross section was presented, considering null geodesics impinging upon a Kerr BH. We can adopt the same treatment for Kerr-Newman BHs, obtaining basically the same formulas presented in Sec. III. B. 1 of Ref. [18].

For an impact vector with components

$$\vec{b} = (b\cos\gamma\cos\chi, b\sin\chi, -b\sin\gamma\sin\chi), \tag{15}$$

we find, for the radial part of the geodesic equation,

$$R(r) = [(r^2 + a^2) - a\mathcal{L}_z]^2 - \Delta[(\mathcal{L}_z - a)^2 + \mathcal{K}], \tag{16}$$

with

$$\mathcal{L}_z = L_z E^{-1} = b\sin\chi\sin\gamma, \tag{17}$$

and

[1]Note that the $m = 0$ mode has been included among the counterrotating modes.

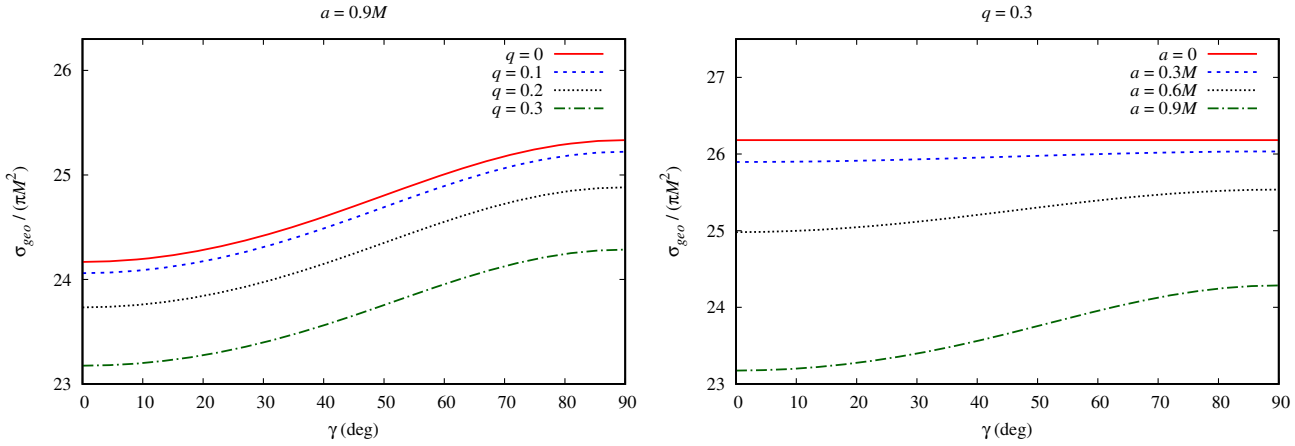

FIG. 2. LEFT: The capture cross section for a fixed value of the rotation parameter ($a = 0.9M$) and different values of the charge-to-mass ratio ($q = 0$, 0.1, 0.2, and 0.3). RIGHT: The capture cross section for a fixed value of the BH charge ($q = 0.3$) and different values of the BH rotation ($a/M = 0$, 0.3, 0.6, and 0.9).

$$\mathcal{K} = KE^{-2} = b^2(\cos^2\chi + \sin^2\chi\cos^2\gamma) - a^2\cos^2\gamma, \quad (18)$$

where K is Carter's constant. In order to find the critical radius and the critical impact parameter, we have to solve $R(r_c) = 0$ and $R'(r_c) = 0$.

The capture cross section is exhibited in Fig. 2 as a function of the null geodesic angle of incidence. We consider different values for the BH rotation parameter (right panel) and electric charge (left panel), showing that the capture cross section diminishes as we increase the values of the Kerr-Newman BH spin and charge-to-mass ratio. For the static case ($a = 0$), the capture cross section is independent of the incidence angle, but for $a > 0$, the capture cross section increases as we increase γ, reaching its maximum value at the equatorial plane ($\gamma = 90$ deg).

IV. RESULTS

Throughout this section, we exhibit an assortment of our numerical results for the massless scalar absorption cross section of Kerr-Newman BHs. In order to obtain our results, we numerically solve Eq. (7) submitted to the boundary conditions given in Eq. (9). Knowing the radial equation solutions, we are able to find the reflection and the transmission coefficients by comparing the numerical solutions with the analytical ones given in Eq. (9) at $r = r_\infty$, where r_∞ represents the numerical infinity.

In Fig. 3 we show the total absorption cross section in the on-axis case ($\gamma = 0$) for a fixed rotation parameter (left panel) and for a fixed BH charge (right panel). In the on-axis case, we note that the absorption cross section presents behavior similar to the static BH case; i.e., the total absorption cross section starts from a value given by its

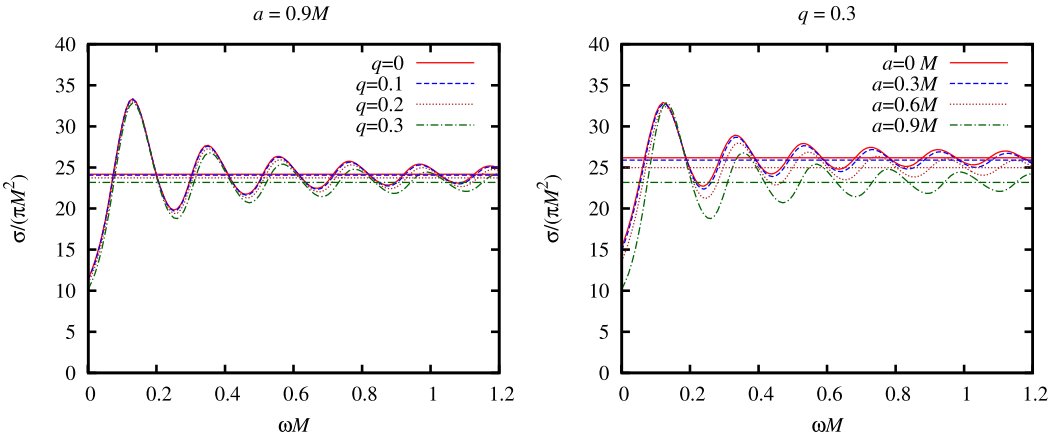

FIG. 3. LEFT: The total absorption cross section for a fixed BH rotation, $a = 0.9M$, with $q = 0$, 0.1, 0.2, and 0.3. RIGHT: The total absorption cross section for a BH charge $q = 0.3$ and different rotation parameters $a/M = 0$, 0.3, 0.6, and 0.9. Both left and right panels were obtained for on-axis incidences ($\gamma = 0$), and the horizontal lines are the capture cross sections of null geodesics in each case.

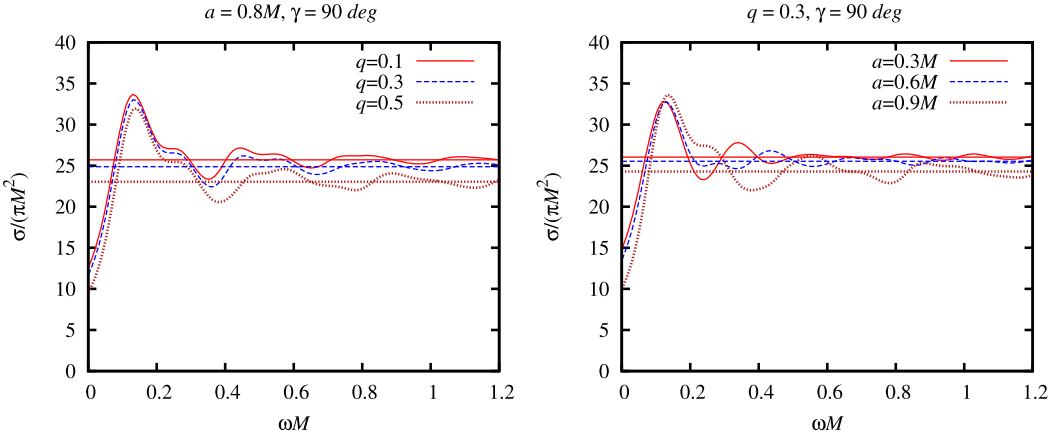

FIG. 4. LEFT: The total absorption cross section for incidences along the equatorial plane for $a = 0.8M$, and $q = 0.1$, 0.3, and 0.5. RIGHT: The total absorption cross section for $\gamma = 90$ deg, with $q = 0.3$, and different BH rotations $a/M = 0.3$, 0.6, and 0.9. The horizontal lines are the values of the capture cross section for null geodesics in each case.

event horizon area and then oscillates with a decreasing amplitude around its high-frequency limit, which is represented by horizontal lines, approaching this value for larger values of ω. Furthermore, we can see that the larger the BH charge is and the faster its spin is, the smaller the total absorption cross section is. This behavior is also observed for the capture cross section of null geodesics (see Fig. 2).

For off-axis incident waves, the oscillating pattern of the absorption cross section is less regular than that of the on-axis case. In order to illustrate this, in Fig. 4, we consider incidences along the equatorial plane $\gamma = 90$ deg. In the left panel of Fig. 4, we choose Kerr-Newmann BHs with a fixed rotation parameter, $a = 0.8M$, and with different charge-to-mass ratios $q = 0.1$, 0.3, and 0.5. We also consider rotating and charged BHs with the same electric charge $q = 0.3$ (right panel) and different rotation parameters $a/M = 0.3$, 0.6, and 0.9. For general behavior, we can observe, in both the left and right panels of Fig. 4, a less regular pattern of the absorption cross section, contrasting with the case of on-axis incidence. As we increase the charge-to-mass ratio, the absorption cross section decreases but maintains its essential shape. On the other hand, as we increase the rotation, the absorption cross section becomes less regular.

In Fig. 5, we show results for the corotating and counterrotating contributions to the total absorption cross section. By examining the corotating and counterrotating modes separately, it is possible to identify a more regular behavior. Also, we see that the contributions of the counterrotating modes to the total absorption cross section are larger than the corotating ones. The corotating modes are more absorbed as either the BH charge or rotation parameter decreases. The counterrotating modes are more absorbed as the BH charge decreases, and the behavior for different rotations depends on the frequency regime. In the low-frequency limit, the absorption cross section for

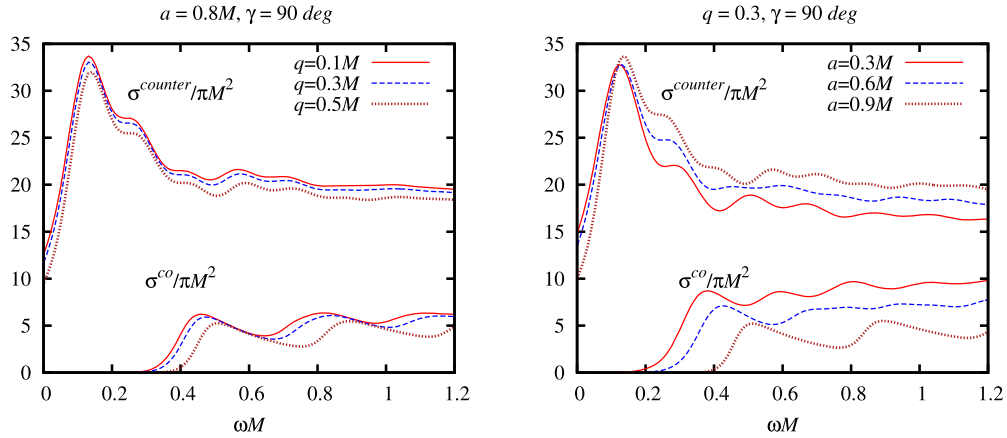

FIG. 5. LEFT: The corotating (σ^{co}) and counterrotating (σ^{counter}) contributions to the absorption cross section for $a = 0.8M$ and $q = 0.1$, 0.3, and 0.5. RIGHT: The corotating and counterrotating contributions to the absorption cross section for $q = 0.3M$ and $a/M = 0.3$, 0.6, and 0.9.

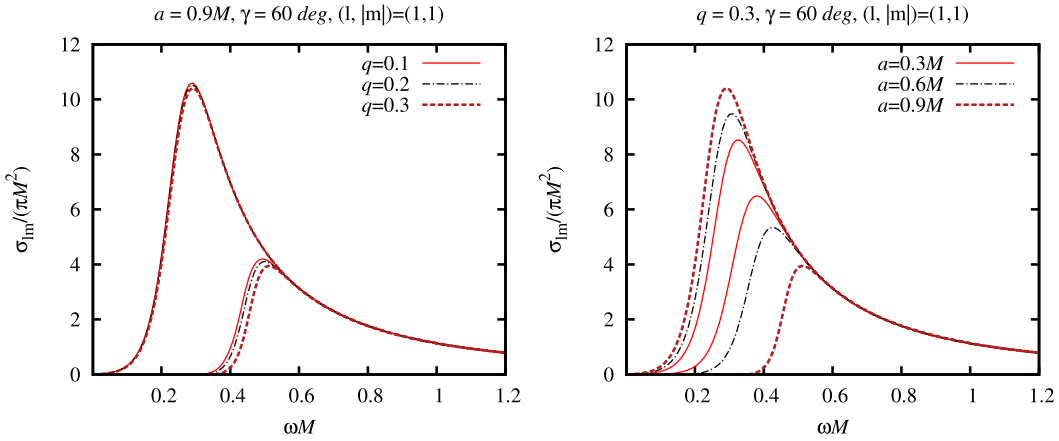

FIG. 6. LEFT: Counterrotating ($m = -1$) and corotating ($m = 1$) partial absorption cross sections for $\gamma = 60$ deg; $a = 0.9M$; and $q = 0.1$, 0.2, and 0.3. RIGHT: Counterrotating and corotating partial absorption cross sections for a fixed BH charge ($q = 0.3$) and different rotation parameters $a/M = 0.3$, 0.6, and 0.9. We consider $\gamma = 60$ deg. In both the right and left panels, the curves associated to the higher peaks are related to the counterrotating modes, while the low peaks are associated to corotating ones.

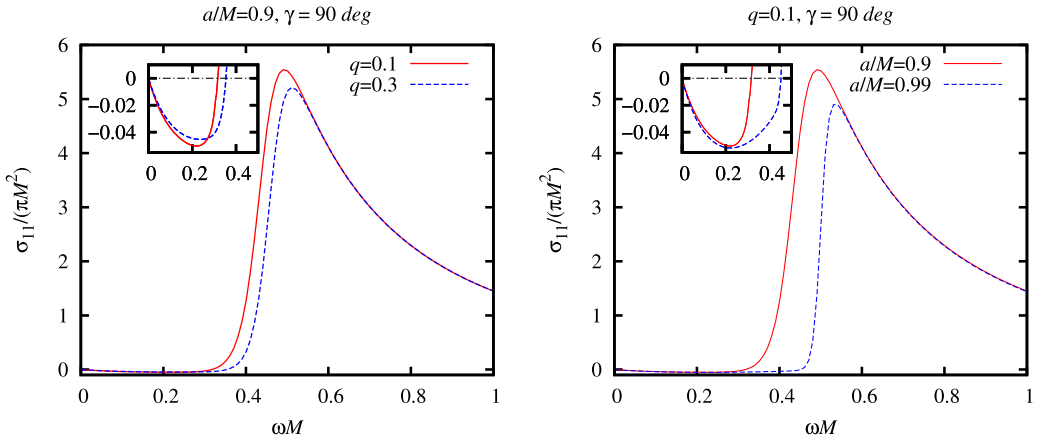

FIG. 7. LEFT: The partial absorption cross section for the mode $l = m = 1$ with $a = 0.9M$, and $q = 0.1$ and 0.3. RIGHT: The partial absorption cross section for the mode $l = m = 1$, with $q = 0.1$, and $a/M = 0.9$ and 0.99. In both the left and right panels, the insets help one see more clearly the superradiance, which is very small for scalar waves.

counterrotating waves decreases as we increase the rotation parameter. In this limit, the absorption cross section is dominated by the waves with $m = 0$ and goes to the area of the black hole as $\omega \to 0$. In the high-frequency regime, $\sigma^{counter}$ increases as a increases.

In Fig. 6, we present the partial absorption cross sections for the dipole mode ($l = 1$). As the BH charge increases, both the corotating ($m = 1$) and counterrotating ($m = -1$) partial cross sections decrease (left panel). On the other hand, as the rotation parameter increases, the associated values of the corotating partial absorption cross section decrease, while the counterrotating ones increase (right panel).

In the Kerr-Newman spacetime, due to superradiance, reflected waves can be amplified, which results in a negative partial absorption cross section. We show the partial absorption cross sections, in Fig. 7, for the mode $l = m = 1$, considering incidence along the equatorial plane, a case for which superradiance is more evident. For a fixed rotation parameter (left panel), the larger the BH charge is, the smaller the superradiance is. On the other hand, as the rotation parameter increases, superradiance increases (right panel).

V. FINAL REMARKS

We have obtained numerically the absorption spectrum of planar massless scalar waves for a Kerr-Newman BH, considering different values for the BH rotation parameter and electric charge. We have confirmed with our numerical results that in the low-frequency regime the absorption cross section tends to the area of the BH horizon, while in the high-frequency regime, it approaches the capture cross section of null geodesics.

We have shown that the absorption cross section presents a regular oscillatory behavior around its high-frequency limit when the waves impinge along the rotation axis ($\gamma = 0$). This oscillatory behavior comes from the contributions of waves with different angular momentum, l. As either the charge or the rotation parameter increases, the absorption cross section decreases, which is consistent with the fact that when we increase these parameters both the area and critical impact parameter of the black hole decrease.

For off-axis incidences ($\gamma \neq 0$), we have observed that the absorption cross section behaves with less regular oscillations around the geometric capture cross section, which is a consequence of the different contributions given by the co- and counterrotating modes. We have also noted that, for off-axis incidences, the oscillatory pattern becomes more irregular for larger values of the BH rotation parameter.

When we consider the corotating and counterrotating contributions to the absorption cross section separately, we identify a more regular absorption profile, and we observe that the counterrotating modes are more absorbed than the corotating ones. Moreover, we have obtained that the larger the BH charge and rotation parameter are, the less absorbed the corotating waves are. For the counterrotating case, we have obtained that the waves are more absorbed as the BH charge decreases, and as we increase the rotation parameter, we have different behaviors for different frequency regimes. This happens because in the low-frequency limit the field is dominated by the modes with $m = 0$, tending to the area of the BH horizon, which decreases as we increase the BH rotation. As we reach higher values of the frequency, the absorption cross section increases for bigger values of the BH rotation parameter.

For the case of superradiant scattering, we found that superradiance is larger the faster the BH spins and the smaller the BH charge is. As for the Kerr case, superradiance yields a negative partial absorption cross section, although the total absorption cross section remains positive.

ACKNOWLEDGMENTS

The authors would like to thank Sam R. Dolan for discussions and acknowledge Conselho Nacional de Desenvolvimento Científico e Tecnológico (CNPq) and Coordenação de Aperfeiçoamento de Pessoal de Nível Superior (CAPES) for partial financial support. L. L. thanks the University of Sheffield for kind hospitality.

[1] S. Bowyer, E. T. Byram, T. A. Chubb, and H. Friedman, Cosmic x-ray sources, Science **147**, 394 (1965).
[2] B. P. Abbott *et al.* (LIGO Scientific and Virgo Collaborations), Observation of Gravitational Waves from a Binary Black Hole Merger, Phys. Rev. Lett. **116**, 061102 (2016).
[3] B. P. Abbott *et al.* (Virgo and LIGO Scientific Collaborations), GW151226: Observation of Gravitational Waves from a 22-Solar-Mass Binary Black Hole Coalescence, Phys. Rev. Lett. **116**, 241103 (2016).
[4] N. G. Sanchez, Absorption and emission spectra of a Schwarzschild black hole, Phys. Rev. D **18**, 1030 (1978).
[5] N. Sánchez, Elastic scattering of waves by a black hole, Phys. Rev. D **18**, 1798 (1978).
[6] E. Jung and D. K. Park, Absorption and emission spectra of an higher-dimensional Reissner-Nordstrom black hole, Nucl. Phys. **B717**, 272 (2005).
[7] L. C. B. Crispino and E. S. Oliveira, Electromagnetic absorption cross section of Reissner-Nordstrom black holes, Phys. Rev. D **78**, 024011 (2008).
[8] L. C. B. Crispino, S. R. Dolan, and E. S. Oliveira, Scattering of massless scalar waves by Reissner-Nordstrom black holes, Phys. Rev. D **79**, 064022 (2009).
[9] L. C. B. Crispino, A. Higuchi, and E. S. Oliveira, Electromagnetic absorption cross section of Reissner-Nordstrom black holes revisited, Phys. Rev. D **80**, 104026 (2009).
[10] E. S. Oliveira, L. C. B. Crispino, and A. Higuchi, Equality between gravitational and electromagnetic absorption cross sections of extreme Reissner-Nordstrom black holes, Phys. Rev. D **84**, 084048 (2011).
[11] C. L. Benone, E. S. de Oliveira, S. R. Dolan, and L. C. B. Crispino, Absorption of a massive scalar field by a charged black hole, Phys. Rev. D **89**, 104053 (2014).
[12] L. C. B. Crispino, S. R. Dolan, A. Higuchi, and E. S. de Oliveira, Inferring black hole charge from backscattered electromagnetic radiation, Phys. Rev. D **90**, 064027 (2014).
[13] L. C. B. Crispino, S. R. Dolan, A. Higuchi, and E. S. de Oliveira, Scattering from charged black holes and supergravity, Phys. Rev. D **92**, 084056 (2015).
[14] C. L. Benone and L. C. B. Crispino, Superradiance in static black hole spacetimes, Phys. Rev. D **93**, 024028 (2016).
[15] C. L. Benone, E. S. de Oliveira, S. R. Dolan, and L. C. B. Crispino, Addendum to absorption of a massive scalar field by a charged black hole, Phys. Rev. D **95**, 044035 (2017).
[16] K. Glampedakis and N. Andersson, Scattering of scalar waves by rotating black holes, Classical Quantum Gravity **18**, 1939 (2001).
[17] S. R. Dolan, Scattering and absorption of gravitational plane waves by rotating black holes, Classical Quantum Gravity **25**, 235002 (2008).
[18] C. F. B. Macedo, L. C. S. Leite, E. S. Oliveira, S. R. Dolan, and L. C. B. Crispino, Absorption of planar massless scalar waves by kerr black holes, Phys. Rev. D **88**, 064033 (2013).

[19] C. F. B. Macedo and L. C. B. Crispino, Absorption of planar massless scalar waves by bardeen regular black holes, Phys. Rev. D **90**, 064001 (2014).
[20] C. F. B. Macedo, E. S. de Oliveira, and L. C. B. Crispino, Scattering by regular black holes: Planar massless scalar waves impinging upon a bardeen black hole, Phys. Rev. D **92**, 024012 (2015).
[21] C. F. B. Macedo, L. C. S. Leite, and L. C. B. Crispino, Absorption by dirty black holes: Null geodesics and scalar waves, Phys. Rev. D **93**, 024027 (2016).
[22] W. Hu, R. Barkana, and A. Gruzinov, Fuzzy Cold Dark Matter: The Wave Properties of Ultralight Particles, Phys. Rev. Lett. **85**, 1158 (2000).
[23] L. Hui, J. P. Ostriker, S. Tremaine, and E. Witten, Ultralight scalars as cosmological dark matter, Phys. Rev. D **95**, 043541 (2017).
[24] S. W. Hawking, Black hole explosions, Nature (London) **248**, 30 (1974).
[25] G. W. Gibbons, Vacuum polarization and the spontaneous loss of charge by black holes, Commun. Math. Phys. **44**, 245 (1975).
[26] S. Davidson, S. Hannestad, and G. Raffelt, Updated bounds on millicharged particles, J. High Energy Phys. 05 (2000) 003.
[27] V. Cardoso, C. F. B. Macedo, P. Pani, and V. Ferrari, Black holes and gravitational waves in models of minicharged dark matter, J. Cosmol. Astropart. Phys. 05 (2016) 054.
[28] C. W. Misner, Interpretation of Gravitational-Wave Observations, Phys. Rev. Lett. **28**, 994 (1972).
[29] A. Higuchi, Low frequency scalar absorption cross-sections for stationary black holes, Classical Quantum Gravity **18**, L139 (2001); Addendum, Classical Quantum Gravity **19**, 599(A) (2002).
[30] M. Abramovitz and I. A. Stegun, *Handbook of Mathematical Functions with Formulas, Graphics and Mathematical Tables* (Cambridge University Press, Cambridge, England, 1964).
[31] R. Brito, V. Cardoso, and P. Pani, *Superradiance: Energy Extraction, Black-Hole Bombs and Implications for Astrophysics and Particle Physics* (Springer, Berlin, 2015), Vol. 906.
[32] L. C. S. Leite, L. C. B. Crispino, E. S. de Oliveira, C. F. B. Macedo, and S. R. Dolan, Absorption of massless scalar field by rotating black holes, Int. J. Mod. Phys. D **25**, 1641024 (2016).